INORGANIC CHEMISTRY FRONTIERS

RESEARCH ARTICLE

View Article Online
View Journal | View Issue

Cite this: *Inorg. Chem. Front.*, 2024, **11**, 2471

Perovskite photoinitiated RAFT-mediated polymerization-induced self-assembly for organic–inorganic hybrid nanomaterials†

Bingfeng Shi,‡[a,b] Wanchao Hu,‡[a] Shiyi Li,[a] Zhinan Xia[a] and Changli Lü *[a]

Perfluorooctanoic acid-modified $CsPbBr_3$ perovskite quantum dots (F-PQDs) are used as both luminescence centers and photocatalysts to prepare organic–inorganic nanohybrid assemblies. Polymerization-induced self-assembly (PISA) technology of poly(poly(ethylene glycol) monomethyl ether methacrylate)-*b*-poly(perfluorooctyl)ethyl methacrylate copolymers (POEGMA-*b*-PFOEMA) *via* photo-induced electron/energy transfer RAFT (PET-RAFT) simplifies the synthetic steps of hybrid nanoparticles and enables the *in situ* encapsulation of PQDs through the dipole–dipole interaction based on the fluorocarbon chain on F-PQDs' surface and FOEMA. The insolubility of the PFOEMA block with liquid crystal properties allows for effective modulation of the hybrid nanostructure in toluene. Modulation of the block length achieves the transition from nanorods to spindle-like nano-assemblies and these hybrid nanoparticles possess PQDs' inherent fluorescence and enhanced stability. This strategy simplifies the preparation scheme of a PQD/polymer composite and provides a new perspective for the design of organic–inorganic hybrid materials through the photo-PISA strategy.

Received 25th January 2024,
Accepted 17th March 2024

DOI: 10.1039/d4qi00233d

rsc.li/frontiers-inorganic

Introduction

Perovskite quantum dots (PQDs) have attracted increasing attention from the materials field based on their outstanding photophysical properties. Meanwhile, the inherent instability of their ionic structure has limited further application.[1–3] A myriad of emerging approaches, including component engineering, ligand engineering, surface engineering, and matrix encapsulation, effectively enhance the stability of PQDs.[4] Nevertheless, the diminishing luminescence in the long-term storage of PQD-based materials owing to the dynamic dissociation of surface ligands and the reduced dispersion by host matrixes is disadvantageous for practical applications.[1] Hybrid assemblies between functional polymers and PQDs offer an ideal solution to these problems.[1–5] Functional polymers, such as amphiphilic polymers,[6] coordination polymers,[7] and zwitterionic polymers,[8,9] can effectively realize microcrosslinking and passivate the perovskite surface, which prevents the dissociation of PQDs. To date, organic–inorganic hybrid materials based on PQDs have been widely used in optoelectronic devices, solar cells, and biomedical fields.[1–3] However, for most PQD/polymer composites, the synthesis and purification of polymers are tedious and complicated; then, it is difficult to construct isotropic nanomaterials, which is adverse for the preparation of high-performance devices and precision instruments.

Nowadays, PQDs are used as photocatalysts (PCs) for photopolymerization as summarized in Table S1.† PQDs also show superb adaptability to a variety of photopolymerizations, including photoinduced radical polymerization,[10–12] PET-RAFT polymerization,[13,14] photoinduced ATRP polymerization,[15] *etc*. In most photopolymerizations, maintaining excellent photoelectron transport properties and luminescence seems to be a paradox, and the photoelectron transfer in the reaction means the occurrence of polymerization and fluorescence quenching. Thus, it is still challenging to strike a balance between the luminescence and polymerization efficiency for the PQD/polymer composite *via* an appropriate strategy.

Polymerization-induced self-assembly (PISA) is one method that can achieve high-content and scalable preparation of block polymer nanoparticles, in which the polymerization and self-assembly processes are highly overlapping. Most PISA processes are realized by thermal polymerization, which may restrict their application in some high-temperature intolerant systems. The groups of Boyer,[16,17] Cai,[18] and Tan[19] introduced

[a]*Institute of Chemistry, Northeast Normal University, Changchun 130024, P. R. China. E-mail: lucl055@nenu.edu.cn*
[b]*Institute of Chemistry, Baotou Teachers College, Baotou 014030, P. R. China*
†Electronic supplementary information (ESI) available: Comments relevant not central to the matter under discussion, limited experimental and spectral data. See DOI: https://doi.org/10.1039/d4qi00233d
‡These authors contributed equally to this work.

photo-RAFT and PET-RAFT technology into PISA, which has effectively expanded the boundaries of PISA at room temperature. In addition, functional block polymer nanoparticles prepared using PISA technology have often been used as templates,[20] nanoreactors,[20] or crystallization centers[21] to achieve a hybrid assembly. However, the range of inorganic nanomaterials used in hybrid assembly is limited, mainly focusing on noble metal nanoparticles and oxides, and most of them require extra initiators. Moreover, it is difficult to achieve the precise positioning of inorganic nanoparticles.[22,23]

Here, we report an efficient strategy to fabricate organic–inorganic hybrid nanomaterials easily by PET-RAFT mediated PISA, achieving the compatibility of stability, polymerization conversion, and luminescence for fabricating PQD/polymer nanohybrids. Perfluoroalkyl chain modified $CsPbBr_3$ PQDs (F-PQDs), which were obtained by ligand exchange between the perfluorooctanoic acid (PFOA) and PQDs, served as both PC and fluorescence centres of the hybrid materials (Scheme 1A and B). The PISA process was carried out in a non-polar solvent (toluene) with poly(poly(ethylene glycol) monomethyl ether methacrylate) (POEGMA) as the macromolecular chain transfer agent (macro-CTA) and 2-(perfluorooctyl)ethyl methacrylate (FOEMA) as the monomer (Scheme 1C).

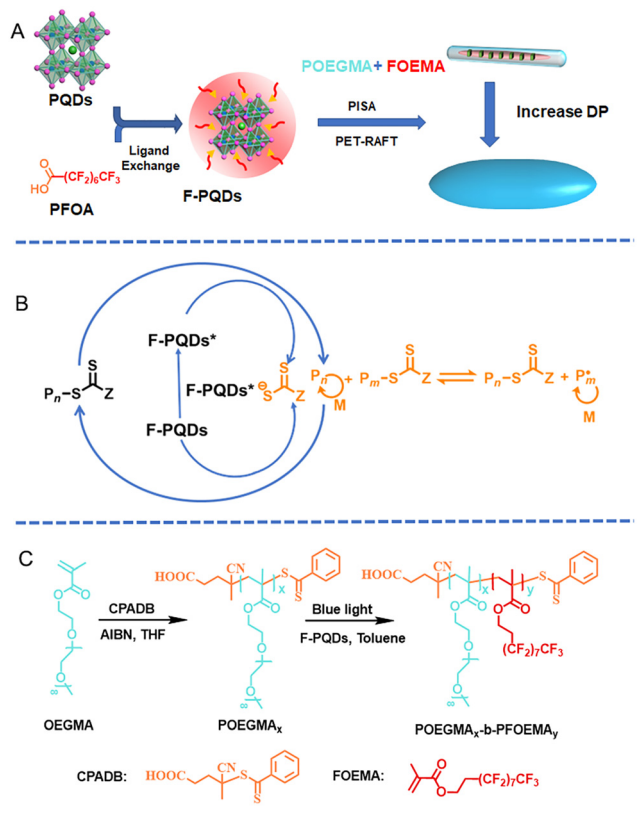

Scheme 1 (A) Schematic demonstration of the surface ligand exchange strategy of PQDs and the PISA process based on PET-RAFT polymerization, (B) the proposed PET-RAFT polymerization mechanism of F-PQDs, and (C) a synthetic approach for producing the diblock copolymer POEGMA-*b*-PFOEMA.

Furthermore, the dipole–dipole interaction between FOEMA and perfluoroalkyl chain on the F-PQD′ surface can promote an efficient package of F-PQDs, enabling the precise positioning of PQDs in the core of the resultant polymer nanohybrid assemblies. The nanohybrid assemblies showcased the transformation from nanorods to spindle-like nanostructures by regulating the degree of polymerization (DP) while maintaining excellent luminescence and enhanced stability.

Results and discussion

$CsPbBr_3$ PQDs with an average size of 12.23 nm were synthesized by the hot-injection method according to Kovalenko's report[24] (Fig. 1A and Fig. S1†) and the F-PQDs were prepared through a ligand exchange method with a reduced average size of around 10.89 nm (Fig. 1B and Fig. S2, S3†). The smaller size of F-PQDs is related to the dissociation–desorption process that occurs during the ligand exchange. Strongly acidic PFOA is more likely to coordinate with PQDs compared with oleic acid (OA), which strips the weakly coordinated ions from the surface of the perovskite.[25] The X-ray diffraction (XRD) patterns of F-PQDs are consistent with those of $CsPbBr_3$ PQDs crystals (JCPDS no. 54-0752), which indicates that the addition of PFOA causes no substantial damage to the crystal form (Fig. S4†). X-Ray photoelectron spectroscopy (XPS) confirmed that the PFOA was successfully archived on the PQD surface after ligand exchange, as the F element bands at 699 eV and 880 eV were identified in the F-PQDs (Fig. 1C).[26] In addition, the appearance of the C–F peak at 291.7 eV in the high-resolution C 1s spectra of F-PQDs also justifies this conclusion (Fig. 1D and Fig. S5†).[26] Enhanced fluorescence of F-PQDs was observed at 508 nm as compared with the PQDs, and the photoluminescence quantum yield (PLQY) of 48% for PQDs increased to 73% for F-PQDs (Fig. 1E and Table S2†). The passivation of surface defects and the exfoliation of low-coordination lead ions may be responsible for this increased intensity, due to the easier coordination interaction between PFOA and PQDs than that of OA. Tang,[27] Isobe,[25] and our previous work[26] showed that the fluorocarbon chain can effectively passivate the PQD surface to improve the PLQY. Thus, compared with the PQDs, the PL lifetime τ_{ave} of F-PQDs decreased, whereas the internal reorganization lifetime τ_1 increased and the surface state reorganization τ_2 dropped, which means that a reduced surface traps may suppress nonradiative transitions (Fig. S6 and Table S2†).[26,28]

Comb-like poly-FOEMA has been widely utilized as a surface modification material based on the low critical surface tension of the fluorocarbon chain (γ_c = 8–11 mN m^{-1}).[29] The phase separation behavior between rigid perfluoroalkyl and hydrocarbon segments can easily form a liquid crystalline (LC) block, making PFOEMA a unique class in the PISA field.[30–32] An's group[30] and Yuan's group[31,32] achieved effective regulation of multiple topological structures driven by the LC block with the PFOEMA unit on the block copolymer through thermal RAFT polymerization, respectively. However, there

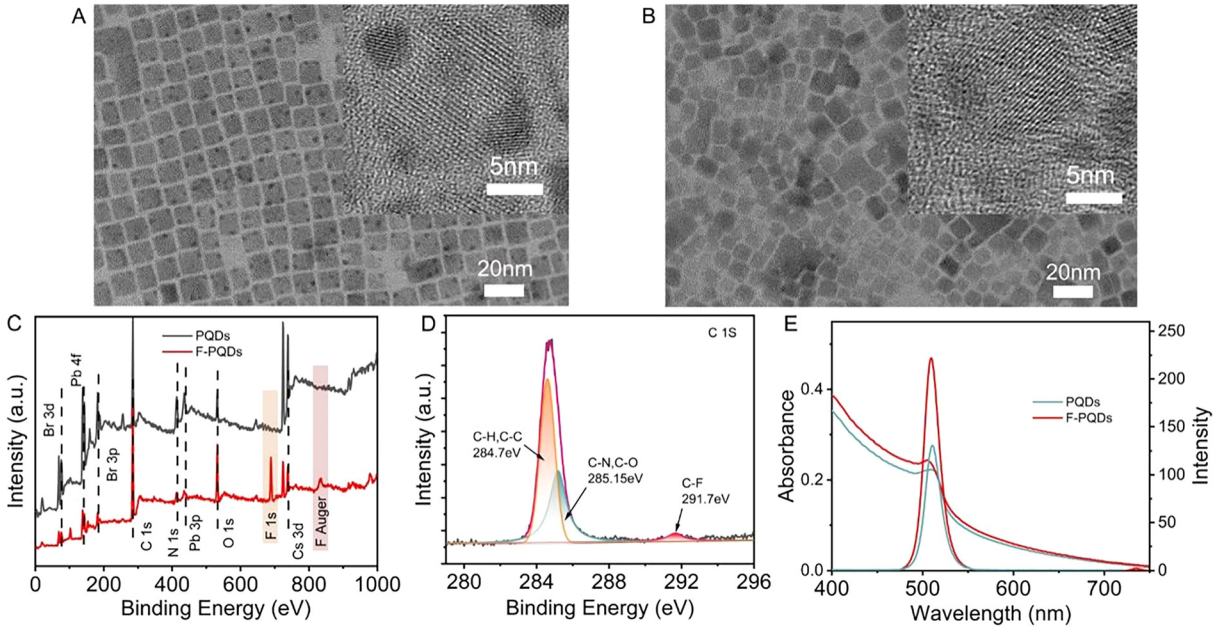

Fig. 1 (A) TEM and HRTEM images of PQDs, (B) TEM and HRTEM images of F-PQDs, (C) XPS spectra of PQDs and F-PQDs, (D) high-resolution C 1s spectra of F-PQDs, and (E) UV-vis absorption spectra and PL spectra (excited at 380 nm) of PQDs and F-PQDs in toluene.

have been no reports on the PET-RAFT polymerization of FOEMA catalyzed by PQD so far. To evaluate the photocatalytic polymerization capability of PQDs and F-PQDs to FOEMA in toluene, a 425 nm blue LED was utilized as the light source and CPADB was selected as the CTA based on it being inactive under this condition.[33] The details of structural determination and calculation of the molecular weight of PFOEMA are described in ESI section 3.3 and Fig. S7.† During the reaction, an increasing number of bright precipitates can be observed (Fig. S8 and S9†). After a 12 h reaction, the conversion of FOEMA reached 18.3% and 26.2% for F-PQDs and PQDs as the photocatalysts (PCs), respectively (Table S3, entries 5 and 6†). Under the same conditions, only very low conversion of the polymerization system without PC was detected, which indicates that PQDs and F-PQDs can effectively catalyze the polymerization of FOEMA, excluding the interference of polymerization initiated by light directly. The FOEMA conversions of F-PQDs and PQDs as the PCs reached 28% and 25%, respectively (Table S3, entries 7 and 8†), when the reaction time was extended to 18 h. Further prolonging the reaction time did not increase the conversion, which is directly related to the precipitation of the polymer and PC during the polymerization process. After washing the precipitate three times, the final materials still maintained bright fluorescence (Fig. S11†). Furthermore, SEM was used to characterize the morphology of the polymerization products (PQDs/PFOEMA and F-PQDs/PFOEMA). We found that PQDs/PFOEMA exhibited a typical nano-microsphere structure, while F-PQD/PFOEMA hybrid materials exhibited an elliptical and a typical nanohybrid assembly morphology (Fig. S12†). Ion–dipole interaction and dipole–dipole interaction might be considered as the origin of this result, which was also confirmed by the previous report of Wang's group.[34] The interaction between the terminated $-CF_3$ group and PQDs promotes polymer grafting onto the PQDs' surface, and the entanglement between perfluoroalkyl chains also accelerates this process.

POEGMA (DP = 78, $Đ$ = 1.18) was synthesized as a macro-CTA for constructing a di-block copolymer with FOEMA as a monomer through PET-RAFT polymerization (Fig. S13 and S14†). Specially designed macro-CTA with a long stabilizer block can effectively promote the conversion of PFMOA. The OEGMA was chosen because its electrically neutral character can avoid interaction between the macro-CTA and PQDs. Toluene shows good compatibility with POEGMA and PQDs. First, we synthesized POEGMA-*b*-PPFOMA as a proof-of-concept study utilizing 1 wt% PQDs as PC, where [FOEMA] : [POEGMA-CTA] = 100 : 1. (More experimental details are provided in ESI sections 5.3 and 5.4†.) When the polymerization reaction was stopped after 24 h, the conversion of FOEMA reached 45% for PQDs as PC (Table S4†). The TEM images confirmed that a spindle-like nanostructure was constructed successfully. In addition, there are many unpacked PQDs that can be easily observed (Fig. S16A†). When the F-PQDs were utilized as the PC, the conversion of PFOEMA reached 52% under the same conditions, but for this polymerization system, we found that the unpacked perovskite basically disappeared and the morphology also appeared as spindle-like nanoparticles (Fig. S16B†). The polymerization reaction has a certain induction period and the free radical concentration is constant within a certain period of time (Fig. S17†). The above result shows that the fluorocarbon chain on F-PQDs' surface can efficiently enhance their encapsulation efficiency in polymers during the photopolymerization. The dipole–dipole interaction between fluorocarbon chains may

promote the enrichment of monomers on the PC's surface and accelerated the progress of polymerization. After enrichment, the repulsion between dipoles may further enhance the polymerization efficiency.[31]

To investigate whether higher-order nano-assembled morphologies were formed within 24 h, we varied the solid content by [FOEMA]:[POEGMA-CTA] = 200:1. Generally, the increase of solid content of PISA system is conducive to the improvement of polymerization efficiency; meanwhile it also means an increase in interparticle interactions favoring morphological evolution.[17] As expected, the monomer conversion of the PISA system with 10 wt% solid content is more effective than that of the 5 wt% solid content system. However, when the solid content is increased to 15 wt%, the conversion of monomer is similar to that at 10 wt%, and when the solid content reaches 20 wt%, the conversion decreases to 16.4% (Fig. 2A). The occurrence of this result may be related to the interaction force between the PC, CTA, and monomer. Solid content is positively correlated with monomer concentration. F-PQDs play a role in both self-assembly and polymerization reaction initiation; notably, they also generate fluorescence for the hybrid. Polymerization may occur primarily in solution and polymer assembly occurs dynamically, driven by dipole–dipole interactions and solvophobic interaction under highly dilute conditions (<1% wt%).[35] In contrast, a high solid-state system exhibited enhanced regularity between the monomer and the PC; polymer chains are more likely to proliferate on the F-PQD surface, which inhibits the electron transfer between F-PQDs and CTA, resulting in the ineffective implementation of the PET-RAFT polymerization photocatalyzed by F-PQDs. Furthermore, the fluorescence intensity of nanoparticles with low DP is higher, as demonstrated in Fig. 2B. The TEM images show that spindle-shaped nanoparticles are formed at solid contents of 5 wt% and 10 wt%. Increasing the solid content to 15 wt% leads to the merging of different nanoparticles, which may account for the decrease in fluorescence intensity. High monomer concentration leads to better encapsulation of the catalyst, resulting in smaller ellipsoidal nanoparticles at 20 wt% solid content (Fig. 2C–J). Some nanorods/nanoparticles are assembled into higher-order microstructures to produce spindle-shaped nanostructure, as can be observed in the samples with 5 wt% and 10 wt% solid contents.

Nanoparticles with different DPs of PFOEMA were prepared and the morphology was observed by TEM to further investigate the nanostructure (Fig. 3, Table S5†). A pure phase of nanorod with an average minor axis at 18.6 nm was observed and the reaction solution was milky when the DP of FOEMA was 34 at 10 wt% solid content (Fig. 3A, B and Fig. S18A†). When the DP increased to 75, a spindle-like structure could be observed with an average length of the short axis of 60 nm and the reaction solution turned muddy (Fig. 3C, D and

A

Entry	PC	[M]:[CTA]	Time (h)	Totally solids content (wt%)	Conv. (%)	DP	$M_{n,NMR}$ (kDa)
1	F-PQDs	200:1	24	5	47.4	94.8	89.7
2	F-PQDs	200:1	24	10	57.9	115.8	100.9
3	F-PQDs	200:1	24	15	58	116	101
4	F-PQDs	200:1	24	20	16.4	38.2	43.6

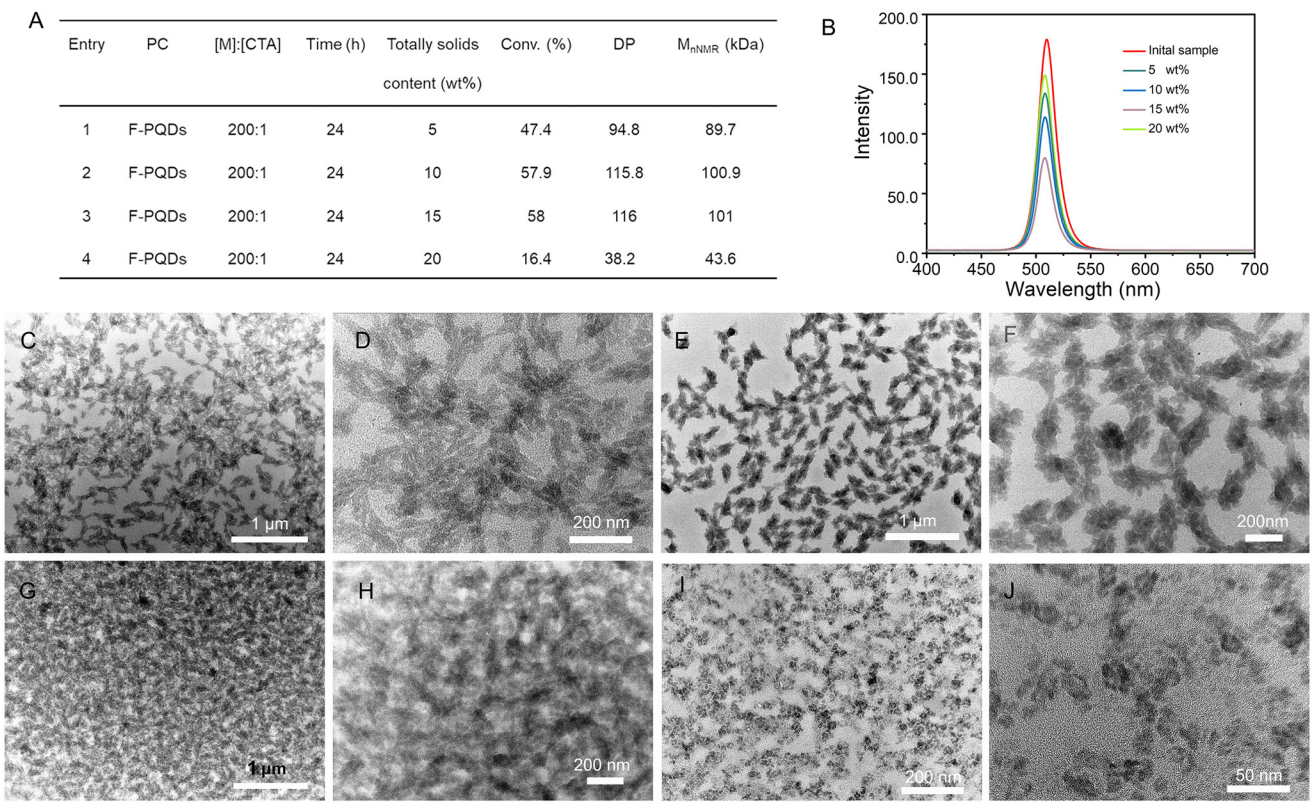

Fig. 2 (A) Characterization of $POEGMA_{78}$-*b*-PFOEMA diblock copolymers synthesized with a different total solid content, (B) PL spectra (excited at 380 nm) of self-assembled POEGMA-*b*-PFOEMA nanoparticles in toluene, and (C–J) TEM images of self-assembled $POEGMA_{78}$-*b*-PFOEMA nanoparticles.

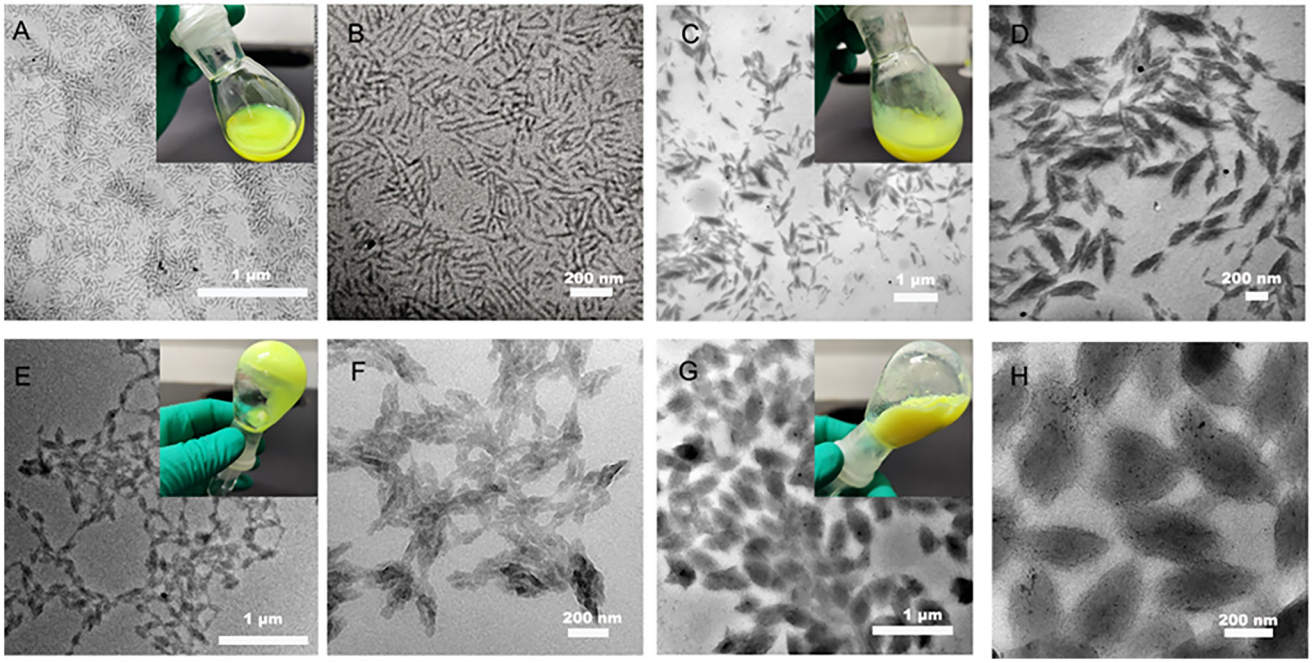

Fig. 3 TEM images of (A and B) POEGMA$_{78}$-*b*-PFOEMA$_{34}$ (conv. = 34%), (C and D) POEGMA$_{78}$-*b*-PFOEMA75 (conv. = 37.5%), (E and F) POEGMA$_{78}$-*b*-PFOEMA$_{137}$ (conv. = 45.6%) and (G and H) POEGMA$_{78}$-*b*-PFOEMA$_{215}$ (conv. = 53.7%) (inset: photographs of sample solutions).

Fig. S18B†). The spindle-shaped nanoparticles become more uniform and the fusion phenomenon of multiple nanoparticles was observed with the increase of DP to 137, and the reaction solution presented a gel-like state (Fig. 3E, F and Fig. S18C†). The fusion between different nanoparticles promoted the formation of uniformly distributed spindles as the DP increased to 215 (Fig. 3G, H and Fig. S18D†). The formation of nanorods may be related to the dipole–dipole interaction between the fluorocarbon chains on the surface of the F-PQDs and the PFOEMA block occupying the dominant position in the assembly, rather than the interfacial tension and the repulsion of the POEGMA corona.[35] Typical spindle-shaped nanoparticles were formed as the polymer chain segment further grew where the LC nature of polymer dominated rather than the interaction between the F-PQDs and the polymer.[30] With the growth of PFOEMA chain segments, the dipole–dipole interactions between POEGMA and PFOEMA blocks increased as well, leading to further particle fusion. An important factor for non-spherical nanoparticles of the assemblies was the formation of an LC phase, which was demonstrated by X-ray diffraction (XRD) and differential scanning calorimetry (DSC). Peaks at 5.65° and 17.3° represent an ordered smectic B phase in Fig. 4A, which means the existence of LC phases.[30,31] The phase transition temperatures of four samples (DP = 34, 75, 137, and 215) in the first heating half-cycle are 90.25 °C, 88.45 °C, 89.72 °C, and 89.33 °C, which are consistent with the previous literature for PFOEMA from LC to liquid solution (Fig. S19–S22†).[30,31] These results indicate that all the nanoparticles prepared by PISA possess LC properties. Elemental mapping of nanoparticles proved the successful embedding of the perovskite (Fig. S23–S26†). All of these nano-assemblies showed excellent fluorescence emission, and the longer lifetimes may be associated with the fusion of different nanocrystals by ligand dissociation and the changed surface environment of the nanocrystals (Fig. 4B, C and Fig. S27, Table S6†).

The above discussion confirms that nanohybrid assemblies with different structures have been successfully synthesized *via* PISA. In addition, another key factor is whether the composite nanoparticles can maintain stable luminescence and achieve improved stability. The aforementioned nano-assemblies (DP = 34, 75, 137, 215) with different morphologies were used for further stability evaluation. A thermal stability test was conducted by heating the solution of samples for a period of time to 70 °C. After 8 h, the brightness of PQDs has almost disappeared, while F-PQDs can still maintain 48% of their original intensity after 12 h. The sample with DP = 34 performed the best among the hybrid nano-assemblies, maintaining 26% of its original brightness after heating for 12 h (Fig. 4D and Fig. S28–S33†). The high thermal stability of F-PQDs can be attributed to the following reasons: (i) PFOA ligands effectively passivate the surface defects of PQDs and (ii) PFOA as a capping ligand effectively inhibits the dissociation of the perovskite structure. Furthermore, the growth of the LC block reduced the thermal stability, which is related to the activation of the LC in the heated state, and the interaction between the fluorine-containing blocks and the chain segments on the F-PQDs' surface promoted the dissociation of the capping ligands. Then, the photostability was studied against UV light irradiation (365 nm, 50 mW) (Fig. 4E and Fig. S34–S39†). The fluorescence intensity of PQDs decreased rapidly and was almost completely quenched within 8 h, while F-PQDs could

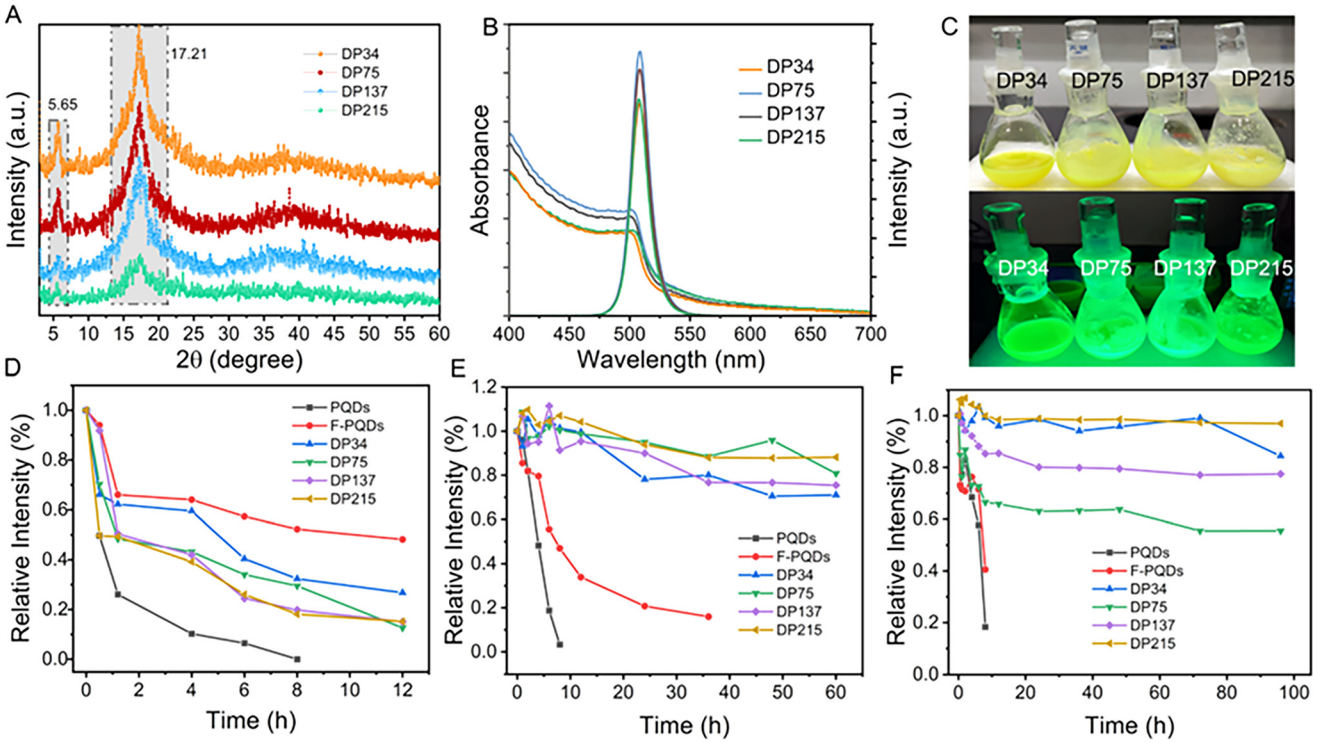

Fig. 4 (A) XRD spectra, (B) UV-vis absorption spectra and PL spectra, and (C) photographs of different samples. The stability of hybrid nano assemblies: (D) thermal stability, (E) UV irradiation stability, and (F) polar solvent stability of different samples.

extend this process to 36 h. In marked contrast, all of the nanohybrid assemblies can be maintained at 80% of the initial intensity after 60 h of irradiation. The nano-assemblies show higher colloidal photostability compared with PQDs and F-PQDs and the photostability increases with the growth of the DP of the FOEMA block, due to the dense LC core effectively limiting ligand dissociation on the PQD surface. The long-term stability of polar solvents was tested with reference to Lin's previous work by adding 10% isopropanol to the solution and stirring vigorously (Fig. 4F and Fig. S40–S45†).[15] The brightness of PQDs and F-PQDs continuously declines within 10 hours when exposed to isopropanol. The sample with DP = 34 can still maintain 55% of their original intensity after 96 h storage, while the sample with DP = 215 performed the best, and 97% of the initial intensity can be maintained. The hybrid assemblies exhibited better stability than PQDs and F-PQDs for polar solvents based on the efficient sequestration of the perovskite QDs by the hydrophobic FOEMA block in the copolymer.

Conclusions

In summary, an efficient strategy to construct organic–inorganic nanohybrid isotropic nanomaterials has been demonstrated, which achieved functional integration and precise control of nanostructures while retaining luminescence of the perovskite/polymer composite, *via* a PISA process. F-PQDs can be served as a photocatalyst for PET-RAFT polymerization mediated PISA and luminous centers for the nano-assemblies. The dipole–dipole interaction force between fluorocarbon chains of ligands on F-PQDs and block copolymer containing PFOEMA block achieves *in situ* encapsulation of the perovskite and the insolubility of LC block enables efficient regulation of nanohybrid structures. The control of the LC segment realizes the effective regulation of the nanostructure from nanorods to ellipsoidal nanohybrid structures, which exhibit great fluorescence emission with enhanced stability. This strategy avoids the tedious steps of constructing PQD/polymer materials and provides a new perspective for the synthesis of organic–inorganic nanohybrid materials through the PISA technique.

Author contributions

B. Shi: conceptualization, investigation, visualization, writing – original draft, and methodology; W. Hu: data curation, software, and formal analysis; S. Li: data curation, software, and formal analysis; Z. Xia: software and visualization; C. Lü: project administration, conceptualization, validation, and writing – review and editing.

Conflicts of interest

There are no conflicts to declare.

Acknowledgements

We would like to acknowledge the financial support of the National Natural Science Foundation of China (22271044) and Jilin Provincial Science and Technology Development Foundation (20210101404JC).

References

1 Q. A. Akkerman, G. Raino, M. V. Kovalenko and L. Manna, Genesis, challenges and opportunities for colloidal lead halide perovskite nanocrystals, *Nat. Mater.*, 2018, **17**, 394–405.
2 A. K. Jena, A. Kulkarni and T. Miyasaka, Halide perovskite photovoltaics: Background, status, and future prospects, *Chem. Rev.*, 2019, **119**, 3036–3103.
3 J. Shamsi, A. S. Urban, M. Imran, L. De Trizio and L. Manna, Metal halide perovskite nanocrystals: Synthesis, post-synthesis modifications, and their optical properties, *Chem. Rev.*, 2019, **119**, 3296–3348.
4 Y. Wei, Z. Cheng and J. Lin, An overview on enhancing the stability of lead halide perovskite quantum dots and their applications in phosphor-converted LEDs, *Chem. Soc. Rev.*, 2019, **48**, 310–350.
5 Y. Huang, T. A. Cohen, B. M. Sperry, H. Larson, H. A. Nguyen, M. K. Homer, F. Y. Dou, L. M. Jacoby, B. M. Cossairt, D. R. Gamelin and C. K. Luscombe, Organic building blocks at inorganic nanomaterial interfaces, *Mater. Horiz.*, 2022, **9**, 61–87.
6 Y. He, Y. Yoon, Y. Harn, G. V. Biesold-McGee, S. Liang, C. H. Lin, V. V. Tsukruk, N. Thadhani, Z. Kang and Z. Lin, Unconventional route to dual-shelled organolead halide perovskite nanocrystals with controlled dimensions, surface chemistry, and stabilities, *Sci. Adv.*, 2019, **5**, eaax4424.
7 V. A. Hintermayr, C. Lampe, M. Low, J. Roemer, W. Vanderlinden, M. Gramlich, A. X. Bohm, C. Sattler, B. Nickel, T. Lohmuller and A. S. Urban, Polymer nanoreactors shield perovskite nanocrystals from degradation, *Nano Lett.*, 2019, **19**, 4928–4933.
8 H. Kim, N. Hight-Huf, J. H. Kang, P. Bisnoff, S. Sundararajan, T. Thompson, M. Barnes, R. Hayward and T. S. Emrick, Polymer zwitterions for stabilization of $CsPbBr_3$ perovskite nanoparticle and nanocomposite films, *Angew. Chem., Int. Ed.*, 2020, **59**, 10802–10806.
9 S. Wang, L. Du, Z. Jin, Y. Xin and H. Mattoussi, Enhanced stabilization and easy phase transfer of $CsPbBr_3$ perovskite quantum dots promoted by high-affinity polyzwitterionic ligands, *J. Am. Chem. Soc.*, 2020, **142**, 12669–12680.
10 Y. C. Wong, J. De Andrew Ng and Z. K. Tan, Perovskite-initiated photopolymerization for singly dispersed luminescent nanocomposites, *Adv. Mater.*, 2018, **30**, e1800774.
11 H. Zhu, M. Cheng, J. Li, S. Yang, X. Tao, Y. Yu and Y. Jiang, Independent dispersed and highly water-oxygen environment stable $FAPbBr_3$ QDs-polymer composite for down-conversion display films, *Chem. Eng. J.*, 2022, **428**, 130974.
12 K. Chen, X. Deng, G. Dodekatos and H. Tuysuz, Photocatalytic polymerization of 3,4-ethylenedioxythiophene over cesium lead iodide perovskite quantum dots, *J. Am. Chem. Soc.*, 2017, **139**, 12267–12273.
13 Y. Zhu, Y. Liu, K. A. Miller, H. Zhu and E. Egap, Lead halide perovskite nanocrystals as photocatalysts for PET-RAFT polymerization under visible and near-infrared irradiation, *ACS Macro Lett.*, 2020, **9**, 725–730.
14 X. Jin, K. Ma, J. Chakkamalayath, J. Morsby and H. Gao, In situ photocatalyzed polymerization to stabilize perovskite nanocrystals in protic solvents, *ACS Energy Lett.*, 2022, **7**, 610–616.
15 S. Liang, S. He, M. Zhang, Y. Yan, T. Jin, T. Lian and Z. Lin, Tailoring charge separation at meticulously engineered conjugated polymer/perovskite quantum dot interface for photocatalyzing atom transfer radical polymerization, *J. Am. Chem. Soc.*, 2022, **144**, 12901–12914.
16 S. Xu, G. Ng, J. Xu, R. P. Kuchel, J. Yeow and C. Boyer, 2-(Methylthio)ethyl methacrylate: a versatile monomer for stimuli responsiveness and polymerization-induced self-assembly in the presence of air, *ACS Macro Lett.*, 2017, **6**, 1237–1244.
17 J. Yeow, J. Xu and C. Boyer, Polymerization-induced self-assembly using visible light mediated photoinduced electron transfer–reversible addition–fragmentation chain transfer polymerization, *ACS Macro Lett.*, 2015, **4**, 984–990.
18 Y. Ding, M. Cai, Z. Cui, L. Huang, L. Wang, X. Lu and Y. Cai, Synthesis of low-dimensional polyion complex nanomaterials via polymerization-induced electrostatic self-assembly, *Angew. Chem., Int. Ed.*, 2018, **57**, 1053–1056.
19 J. He, J. Cao, Y. Chen, L. Zhang and J. Tan, Thermoresponsive block copolymer vesicles by visible light-initiated seeded polymerization-induced self-assembly for temperature-regulated enzymatic nanoreactors, *ACS Macro Lett.*, 2020, **9**, 533–539.
20 B. Shi, H. Zhang, Y. Liu, J. Wang, P. Zhou, M. Cao and G. Wang, Development of ICAR ATRP-based polymerization-induced self-assembly and its application in the preparation of organic-inorganic nanoparticles, *Macromol. Rapid Commun.*, 2019, **40**, e1900547.
21 A. Hanisch, P. Yang, A. N. Kulak, L. A. Fielding, F. C. Meldrum and S. P. Armes, Phosphonic acid-functionalized diblock copolymer nano-objects via polymerization-induced self-assembly: Synthesis, characterization, and occlusion into calcite crystals, *Macromolecules*, 2015, **49**, 192–204.
22 E. J. Cornel, J. Jiang, S. Chen and J. Du, Principles and characteristics of polymerization-induced self-assembly with various polymerization techniques, *CCS Chem.*, 2021, **3**, 2104–2125.
23 B. Niu, Y. Chen, L. Zhang and J. Tan, Organic–inorganic hybrid nanomaterials prepared via polymerization-induced self-assembly: Recent developments and future opportunities, *Polym. Chem.*, 2022, **13**, 2554–2569.

24 L. Protesescu, S. Yakunin, M. I. Bodnarchuk, F. Krieg, R. Caputo, C. H. Hendon, R. X. Yang, A. Walsh and M. V. Kovalenko, Nanocrystals of cesium lead halide perovskites (CsPbX(3), X = Cl, Br, and I): Novel optoelectronic materials showing bright emission with wide color gamut, *Nano Lett.*, 2015, **15**, 3692–3696.

25 D. Sato, Y. Iso and T. Isobe, Effective stabilization of perovskite cesium lead bromide nanocrystals through facile surface modification by perfluorocarbon acid, *ACS Omega*, 2020, **5**, 1178–1187.

26 B. Shi, J. Lü, Y. Liu, Y. Xiao and C. Lü, Ultra-stable water-dispersive perovskite QDs encapsulated by triple siloxane coupling agent system with different hydrophilic/hydrophobic properties, *Mater. Chem. Front.*, 2021, **5**, 4343–4354.

27 Z. Li, Q. Hu, Z. Tan, Y. Yang, M. Leng, X. Liu, C. Ge, G. Niu and J. Tang, Aqueous synthesis of lead halide perovskite nanocrystals with high water stability and bright photoluminescence, *ACS Appl. Mater. Interfaces*, 2018, **10**, 43915–43922.

28 H. Huang, A. S. Susha, S. V. Kershaw, T. F. Hung and A. L. Rogach, Control of emission color of high quantum yield $CH_3NH_3PbBr_3$ perovskite quantum dots by precipitation temperature, *Adv. Sci.*, 2015, **2**, 1500194.

29 Q. Wang, Q. Zhang, X. Zhan and F. Chen, Low surface energy polymer with fluorinated side group, *Prog. Chem.*, 2009, **21**, 2183–2187.

30 L. Shen, H. Guo, J. Zheng, X. Wang, Y. Yang and Z. An, RAFT polymerization-induced self-assembly as a strategy for versatile synthesis of semifluorinated liquid-crystalline block copolymer nanoobjects, *ACS Macro Lett.*, 2018, **7**, 287–292.

31 M. Huo, G. Song, J. Zhang, Y. Wei and J. Yuan, Nonspherical liquid crystalline assemblies with programmable shape transformation, *ACS Macro Lett.*, 2018, **7**, 956–961.

32 M. Huo, D. Li, G. Song, J. Zhang, D. Wu, Y. Wei and J. Yuan, Semi-fluorinated methacrylates: A class of versatile monomers for polymerization-induced self-assembly, *Macromol. Rapid Commun.*, 2018, **39**, e1700840.

33 J. Xu, S. Shanmugam, N. A. Corrigan and C. Boyer, in *Controlled radical polymerization: mechanisms*, 2015, pp. 247–267, DOI: **10.1021/bk-2015-1187.ch013**.

34 Y. Liu, T. Chen, Z. Jin, M. Li, D. Zhang, L. Duan, Z. Zhao and C. Wang, Tough, stable and self-healing luminescent perovskite-polymer matrix applicable to all harsh aquatic environments, *Nat. Commun.*, 2022, **13**, 1338.

35 X. Li, B. Jin, Y. Gao, D. W. Hayward, M. A. Winnik, Y. Luo and I. Manners, Monodisperse cylindrical micelles of controlled length with a liquid-crystalline perfluorinated core by 1D "self-seeding", *Angew. Chem., Int. Ed.*, 2016, **55**, 11392–11396.

